

AEGIS: Radio and Mid-infrared Selection of Obscured AGN Candidates

S. Q. Park¹, P. Barmby², G. G. Fazio¹, K. Nandra³, E. S. Laird³, A. Georgakakis³,
D. Rosario⁴, S. P. Willner¹, G. H. Rieke⁵, M. L. N. Ashby¹, R. J. Ivison⁶, A. L. Coil^{5,7},
S. Miyazaki⁸

ABSTRACT

The application of multi-wavelength selection techniques is crucial for discovering a complete and unbiased set of Active Galactic Nuclei (AGNs). Here, we select a sample of 72 AGN candidates in the Extended Groth Strip (EGS) using deep radio and mid-infrared data from the Very Large Array (VLA) and the *Spitzer Space Telescope*, and analyze their properties across other wavelengths. Only 30% of these sources are detected in deep 200 ks *Chandra X-ray Observatory* pointings. The X-ray detected sources demonstrate moderate obscuration with column densities of $N_{\text{H}} \gtrsim 10^{22} \text{ cm}^{-2}$. A stacked image of sources undetected by *Chandra* shows low levels of X-ray activity, suggesting they may be faint or obscured AGNs. Less than 40% of our sample are selected as AGNs with optical broad lines, mid-infrared power laws, or X-ray detections. Thus, if our candidates are indeed AGNs, the radio/mid-infrared selection criteria we use provide a powerful tool for identifying sources missed by other surveys.

Subject headings: galaxies: active — infrared: galaxies – radio continuum: galaxies – X-rays: galaxies

¹Harvard-Smithsonian Center for Astrophysics, 60 Garden Street, Cambridge, MA 02138, USA; spark@cfa.harvard.edu.

²Department of Physics & Astronomy, University of Western Ontario, London, ON N6A 3K7, Canada.

³Astrophysics Group, Imperial College London, Blackett Laboratory, Prince Consort Road, London SW7 2AZ, United Kingdom.

⁴UCO/Lick Obs., Univ. of California Santa Cruz, 1156 High St., Santa Cruz, CA 95064, USA.

⁵Steward Observatory, University of Arizona, 933 N. Cherry Avenue, Tucson, AZ 85721, USA.

⁶UK Astron. Technology Ctr., Royal Obs., Blackford Hill, Edinburgh EH9 3HJ, United Kingdom.

⁷Hubble Fellow.

⁸Subaru Telescope, National Astronomical Observatory of Japan, 650 North A'ohoku Place, Hilo, HI 96720, USA.

1. INTRODUCTION

Active Galactic Nuclei (AGNs) are sources of tremendous energy that provide clues to the accretion history of the Universe. Defining a complete and reliable sample of AGNs is of great importance in our understanding of how black holes grow over cosmic time as well as the physical processes behind these powerful objects. X-ray emission is an efficient means of detecting energetic activity in distant galactic cores and is often used to find AGN samples (Mushotzky 2004). However, this approach is less successful at finding sources hidden by extreme columns of gas and dust, and models of the observed hard X-ray background require larger numbers of AGNs than are currently observed. Worsley et al. (2005) found that only 50% of the X-ray background is resolved at > 8 keV, and the missing component of the background is consistent in spectral shape with a population of obscured AGNs at redshifts $z \sim 0.5 - 1.5$ with $N_{\text{H}} \sim 10^{23} - 10^{24} \text{ cm}^{-2}$. These synthesis models predict that at 30 keV, the peak of the hard X-ray spectrum, the X-ray background is dominated by heavily obscured sources and obscured AGNs outnumber unobscured AGNs by a ratio of three or four to one (Ueda et al. 2003; Gilli et al. 2007; Treister et al. 2005; Comastri et al. 2001). Thus, the bulk of the accretion in the Universe is taking place in obscured environments that are likely to be missed by X-ray selection methods, highlighting the need for a multi-wavelength approach to build an unbiased census of AGNs.

Mid-infrared and radio surveys provide a way of searching for these elusive obscured nuclei, as these wavelengths are much less affected by extinction and can penetrate through the dusty atmospheres surrounding the AGN. X-ray obscured AGNs are often bright in the mid-IR as the dusty environment surrounding the accretion disk reprocesses incident X-rays from the central engine and re-radiates these photons at infrared wavelengths. Efforts to select AGN candidates with infrared data have mainly concentrated on using mid-IR color criteria (e.g., Lacy et al. 2004; Stern et al. 2005) or power-law selection techniques (e.g., Alonso-Herrero et al. 2006; Barmby et al. 2006). Recently, Daddi et al. (2007) and Fiore et al. (2007) presented evidence of finding Compton thick AGN candidates ($N_{\text{H}} > 10^{24}$) by searching for sources with large mid-IR excess.

Successful attempts have also been made to find obscured AGNs with combined analyses of mid-IR and radio data sets. Donley et al. (2005) found a minimum 4:1 ratio of obscured (Compton thin and Compton thick) to unobscured AGNs in the *Chandra* Deep Field-North (CDF-N) by analyzing sources with radio excess. Martínez-Sansigre et al. (2005) found a 2–3:1 ratio using a combination of mid-IR, near-IR, and radio flux density criteria in the *Spitzer* First Look Survey (FLS) and the Subaru XMM-Newton Deep Field (SXDF). Both results are within model predictions of the obscured AGN ratio. Here, we combine and compare the procedures introduced by these two radio/mid-IR selection techniques to find a

sample of 72 AGN candidates in the Extended Groth Strip (EGS) and use multi-wavelength data to cross-identify their active status. In particular, understanding the X-ray properties of the candidate AGNs is important to control any residual contamination by non-AGNs as well as to study their obscuration and thus put more constraints on the X-ray background. Throughout this paper, we adopt Λ cold dark matter cosmology with $H_0 = 70 \text{ km s}^{-1} \text{ Mpc}^{-1}$, $\Omega_M = 0.3$, and $\Omega_\Lambda = 0.7$.

2. OBSERVATIONS AND DATA REDUCTION

The Extended Groth Strip (EGS) is an approximately 2° by $15'$ region centered on $\alpha = 14^h 17^m$ and $\delta = +52^\circ 30'$. The region's high ecliptic and Galactic latitudes make it ideal for studying extragalactic sources with little Galactic contamination, attracting deep coverage of the field in all wavelengths from radio to X-ray. It is a unique field in its combination of size and depth: it is shallower but larger than the combined GOODS fields, and smaller but deeper than the COSMOS field at most wavelengths. Thus, the intermediate position of the EGS in both depth and area makes it an ideal dataset for combining the AGN selection techniques previously tested in different regimes. Davis et al. (2007) give a detailed description of the region and the All-Wavelength Extended Groth Strip International Survey (AEGIS) data sets.

The radio data were observed at 1.4 GHz using the Very Large Array (VLA) with ~ 18 hr of data per sky position and a resulting source sensitivity limit of $50 \mu\text{Jy}$ (Ivison et al. 2007). The data have a noise level of $10 \mu\text{Jy beam}^{-1}$ and a FWHM of $\sim 3.8''$. Sources were defined by searching signal-to-noise ratio images using the SAD detection algorithm; the technique is outlined in Biggs & Ivison (2006). The infrared properties were found using instruments aboard the *Spitzer Space Telescope* (Werner et al. 2004), with 1.2 ks observations from the Multiband Imaging Photometer (MIPS, Rieke et al. 2004) and 9.1 ks exposures from the Infrared Array Camera (IRAC, Fazio et al. 2004). The *Spitzer* data were processed with the MIPS Instrument Team Data Analysis Tool and the Spitzer Science Center IRAC pipeline, and sources were identified using DAOPHOT. Further details for the MIPS data are provided by Engelbracht et al. (2007) and for the IRAC data by Barmby et al. (2008). The 5σ limiting point-source flux densities of the infrared data are $83 \mu\text{Jy}$ for the $24 \mu\text{m}$ MIPS band and $2 \mu\text{Jy}$ for the $3.6 \mu\text{m}$ IRAC band. Their FWHMs are $5.9''$ and $1.8''$ at $24 \mu\text{m}$ and $3.6 \mu\text{m}$, respectively.

The radio and infrared catalogs were matched to each other using a $2''.5$ search radius. The overlapping VLA and MIPS images result in a field of view of $\sim 0.35 \text{ deg}^2$, with roughly 630 and 9,800 sources at 1.4 GHz and $24 \mu\text{m}$, respectively. In this shared area, there are

482 sources with both 1.4 GHz and 24 μm detections; these sources form the parent sample for our selection. This paper uses two radio/mid-IR selection techniques, one of which also requires use of the 3.6 μm data. Due to a small offset in angle between the IRAC and MIPS images, the IRAC field does not extend as far north as the MIPS and radio fields. Thus, only 325 of the sources detected in both 1.4 GHz and 24 μm are within the IRAC field of view; 321 of these have 3.6 μm counterparts. (The remaining four sources are visible on the IRAC image but were not extracted by DAOPHOT.)

After selecting our candidates, we analyzed their properties using 200 ks X-ray data from the ACIS-I instrument on the *Chandra X-ray Observatory*. The X-ray image is aligned with the IRAC field and thus does not completely cover the VLA/MIPS shared area. Data reduction methods are described by Nandra et al. (2007 in prep). We also utilize R band photometry covering the entire field to a 5σ limiting AB magnitude of ~ 26.5 from the Suprime camera on the Subaru telescope (S. Miyazaki 2005, private communication). Supplemental R band photometry from the Canada-France-Hawaii Telescope (limiting AB magnitude = 24.2 at 8σ ; Coil et al. (2004)) was used in a few cases where the Subaru data lacked coverage. Finally, we use redshifts obtained by the DEEP2 survey, available in two-thirds of the VLA/MIPS shared field from the Keck DEIMOS spectrometer (Davis et al. 2003). The median redshift for the survey is $z \sim 0.7$; redshift measurements for the candidate sources ranged from $z \sim 0.9 - 1.4$. Because the optical fields are quite crowded, sources with multiple potential counterparts within $2''.5$ were checked by eye. Two optical counterparts were thrown out because the match could not be determined unambiguously.

3. AGN SELECTION TECHNIQUES

Two different samples of radio/mid-IR AGN candidates were selected using two separate sets of criteria, as illustrated in Figure 1. The first method, which we refer to as “ q -selection”, relies on the radio/infrared relation for star-forming galaxies and AGNs (Condon 1992). Recent findings have suggested that the relation may break down at high redshift (Kovács et al. 2006; Vlahakis et al. 2007), but Seymour et al. (2007) show that the correlation holds to at least $z \sim 3$. Their study compares observed 1.4 GHz with observed 450 and 850 μm flux densities, which at the redshifts of interest ($z > 1.5$) sample rest wavelengths in the radio near 5 GHz and in the far infrared near 150 and 300 μm . Appleton et al. (2004) defined $q = \log(S_{24 \mu\text{m}}/S_{1.4 \text{ GHz}})$ and showed that $q = 0.84 \pm 0.28$ for non-K-corrected normal star-forming galaxies. Donley et al. (2005) suggested that sources with strong radio emission relative to their 24 μm flux densities are likely to be dominated by AGNs rather than star formation and analyzed a sample of candidate AGNs by selecting sources with $q < 0$. Of the

482 sources detected at both 1.4 GHz and 24 μm in our field, 51 have $q < 0$. We discarded three sources that had flux errors too large to yield convincing ratios of $q < 0$. A fourth source was discarded because the radio detection had only a marginal 24 μm counterpart ($d = 2''.47$) and there were too many possible optical counterparts to be confident in the match. The q -selection only requires the use of the VLA and MIPS parent sample. Unlike the sample of Donley et al. (2005), we require all our candidates to have a detection in the 24 μm band in order to better compare with the second selection technique of this paper. Because of the offset between the MIPS and IRAC images, 35% of these sources lie outside the IRAC field, and 20% are outside the *Chandra* field.

The q -selected sample should include few if any starburst contaminants: adopting $\sigma = 0.28$ at $z = 0$ from Appleton et al. (2004), a threshold of $q < 0$ selects sources 3.4 standard deviations below the average q value expected for starbursts. This difference may even be a conservative estimate, as Boyle et al. (2007) find a higher $q = 1.39 \pm 0.02$ for starbursts using stacked data in the *Spitzer* Wide Field Survey (SWIRE). Donley et al. (2005) and Seymour et al. (2007) show that at higher redshifts, the difference in q should remain constant or increase when comparing LINERs, Seyfert 2s and spiral galaxies to starburst systems. The q values of ULIRGs will fall closer to our selection limit with increasing redshift, though their values should remain above our cut of $q = 0$ out to $z \gtrsim 2.5$. At such high redshifts, even our faintest candidates would have radio luminosities too high to be consistent with starburst systems, and we do not expect our sample to be contaminated with such non-AGN sources.

The second selection method, hereafter referred to as the “flux-cut” method, employs the 3.6 μm data set in addition to the 24 μm and 1.4 GHz parent population to identify an AGN-rich sample. The selection is designed to find obscured AGNs near $z \sim 2$ and is thus a good complement to the lower- z q -selection technique. The redshift calculation comes from assuming the 3.6 μm emission will be dominated by the old stellar population and forming a 3.6 μm - z relation (Martínez-Sansigre et al. 2005), analogous to the K - z relation for radio galaxies (Willott et al. 2003). The relation assumes the galaxies have an elliptical host galaxy, which would not be the case for potential starburst contaminants. However, comparing the relation with local galaxy templates revealed that the correlation (and thus, the redshift assumption) remained valid even for reddened ULIRG templates. The flux-cut method is outlined in detail by Martínez-Sansigre et al. (2005, 2007). We adopted their flux limits:

- (i) $S_{24 \mu\text{m}} > 300 \mu\text{Jy}$
- (ii) $100 \mu\text{Jy} \leq S_{1.4 \text{ GHz}} \leq 2 \text{ mJy}$
- (iii) $S_{3.6 \mu\text{m}} \leq 45 \mu\text{Jy}$

The 24 μm selection was chosen to find a flux density limited sample of active galaxies; a flux density of 300 μJy at $z = 2$ corresponds to quasars of luminosity $L \geq 0.2L_{\text{quasar}}^*$ at rest-frame 8 μm . At these wavelengths, dust extinction is negligible except in extreme cases. In AGN unification schemes, a dusty torus surrounds the optically and X-ray bright accretion disk. Dust particles absorb and re-emit these photons, and a torus viewed edge-on would therefore be optically/X-ray obscured but *bright* in the mid-IR. Weedman et al. (2006) and Brand et al. (2006) show that the AGN fraction tends to increase as 24 μm flux density increases. Accepting only higher flux density sources should therefore improve our probability of finding AGNs.

At $z \sim 2$, the MIPS criterion alone may select star-forming systems with strong PAH features. The minimum radio flux density cut is designed to eliminate these starburst systems. Using the lower limit of 100 μJy from Martínez-Sansigre et al. (2007) rather than the 350 μJy limit of Martínez-Sansigre et al. (2005) increases our sample size while still being high enough to avoid nearly all starburst contaminants. Using the equations for star-forming rates from Yun et al. (2001) and Wu et al. (2005), if we assume that the 24 μm emission of 300 μJy arises solely from star-forming systems at $z \sim 2$, we would expect a radio flux density that is still an order of magnitude lower than 100 μJy . The upper limit of the radio criterion removes extreme radio-loud sources whose potential jets may complicate the analysis; only one potential flux-cut candidate is omitted by this upper limit (see Figure 1). From the parent sample of 482 sources, 184 fit these MIPS and radio flux criteria.

The 3.6 μm criterion weeds out unobscured AGNs and corresponds to a rest frame wavelength of 1.2 μm at $z = 2$. Dust extinction makes the near-IR emission of obscured AGNs much fainter than that of unobscured sources. Requiring high 24 μm flux densities and low 3.6 μm flux densities focuses the sample on obscured types. Out of the 184 sources that fit the 24 μm and 1.4 GHz criteria, 115 are within the IRAC field. Of those, the 3.6 μm criterion yields a final sample size of 28 flux-cut sources. We compared the radio/24 μm ratios of these sources with the values expected from local ULIRG templates and analyzed their SEDs and multi-wavelength properties. The results suggested only 2-3 potential starburst candidates among the sources; these few interlopers should not alter our results.

We combined both of these techniques to arrive at our final sample. Because we are likely probing different redshift regimes and obscuration levels between the two techniques, only three sources overlap between the 47 q -selected sources and the 28 flux-cut sources. Our final sample thus contains 72 radio/mid-IR AGN candidates (see Table 1).

4. MULTI-WAVELENGTH PROPERTIES

4.1. X-Ray Properties

Thirty-seven of the 47 q -selected sources are within the *Chandra* field; 15 (41%) have X-ray detections with Poisson false probability $< 10^{-3}$ (corresponding to slightly above 3σ in Gaussian statistics) in at least one X-ray band. Of the 28 flux-cut sources, 26 lie within the X-ray image, and four have X-ray counterparts (15%). (The detection rates are only 32% and 12% for the q -selection and flux-cut methods in the higher significance AEGIS-X catalogs (Nandra et al. 2007, in prep), which require a more stringent Poisson cut of $< 4 \times 10^{-6}$.) In comparison, Donley et al. (2005) employed the q -selection method in the CDF-N, where VLA and MIPS observations are similar in depth to ours but *Chandra* X-ray exposures exceed 1 Ms. They found an X-ray counterpart detection rate of 40% at Poisson probability $< 3 \times 10^{-7}$ (5σ), and the rate rises to nearly 80% for probability $< 2 \times 10^{-2}$ (2σ) detections. Martínez-Sansigre et al. (2007) detected $\gtrsim 5\%$ of their flux-cut-selected candidates with a flux limit $F_{2-12 \text{ keV}} = 3 \times 10^{-15} \text{ ergs cm}^{-2} \text{ s}^{-1}$ in the shallower SXDF with XMM exposures of $< 100 \text{ ks}$. They were able to increase the detection fraction to 17% by fitting SEDs to filter out contaminants, a procedure we do not adopt here.

As expected, deeper surveys are required to detect X-ray counterparts to greater completion. Although the *Chandra* data in the EGS comprise the third deepest *Chandra* survey to date, 70% of our sources lack counterparts at the 200 ks depth. This may be due in part to the relative depth of the *Spitzer* data versus the *Chandra* field (see Figure 2). In the EGS, over 50% of the X-ray sources in the field have MIPS counterparts, but only 5% of the MIPS sources have X-ray counterparts. However, some of the undetected sources have upper limits that are greater than the fluxes of the actual detected sources, and often lie on relatively shallow (off-axis) areas of the X-ray map. These sources would likely have been detected with deeper data or on-axis pointings.

X-ray hardness ratios are often used to study AGN type, as harder spectra generally indicate more obscuration. All four X-ray sources in the flux-cut method were detected only in the soft band, whereas 11 of the 15 sources detected with the q -selection method had both hard and soft band detections. Two other q -selected sources were detected only in the soft band, one was detected only in the hard band, and the final source was barely detected in the full band but had neither hard nor soft band detections at our limits. Excluding the source with a full band only detection, the q -selected sources have a mean hardness ratio of -0.19 ($\text{HR} = \text{H} - \text{S} / \text{H} + \text{S}$, where $\text{H} = 2 - 7 \text{ keV}$ counts and $\text{S} = 0.5 - 2 \text{ keV}$ counts).

As measured by hardness ratios, one-third of the X-ray detected q -selected sources are obscured according to the division chosen by Szokoly et al. (2004), who classify obscured

AGNs as those having $HR > -0.2$ in the *Chandra* Deep Field South. Our obscured fraction would rise if we include q -selected sources not detected in X-ray. Assuming all X-ray undetected sources are obscured would yield a maximum obscuration fraction of 73%. At $z = 1$, we derive X-ray luminosities of 10^{42} to 10^{44} ergs/s from the observed fluxes of the detected sources. At this redshift, an obscuration fraction of 73% would be within the limits of Szokoly et al. (2004), who found 45%–75% of their sources to be obscured in the same X-ray luminosity range.

Overall, the combined AGN candidates we find tend to have *softer* hardness ratios than the general sample of X-ray sources in the AEGIS-X catalog. Including the four soft flux-cut sources with the q -selected sources, the mean hardness ratio falls to -0.37 , while the total X-ray population has a mean $HR = -0.17$. The general population of sources with both X-ray and radio detections are even harder with a mean $HR = -0.12$. However, a lack of hard band detection is not necessarily an indication that the source has a soft spectrum, especially for faint sources at higher redshifts (Laird et al. 2006). Also, the q -selected AGNs generally have fluxes comparable to the entire X-ray sample, with an average flux $F_{2-10 \text{ keV}} = 8.3 \times 10^{-15}$ ergs $\text{cm}^{-2} \text{ s}^{-1}$ in the hard band and $F_{0.5-2 \text{ keV}} = 2.7 \times 10^{-15}$ ergs $\text{cm}^{-2} \text{ s}^{-1}$ in the soft band. On the other hand, the flux-cut sources are fainter by a factor of 10 in the soft band (and not detected at all in the hard band). This weaker emission, coupled with the expectation that these flux-cut sources should be near $z \sim 2$, suggests that the sources might be too faint for hard band detections, and spectral fitting is necessary to determine their true spectral slopes.

Two of the X-ray counterparts with soft and hard band detections have spectroscopic redshifts; both of these are obscured with column densities $\gtrsim 10^{22} \text{ cm}^{-2}$, assuming a power-law model⁹ with intrinsic $\Gamma = 1.9$ (e.g. Nandra et al. 1997). Nine X-ray counterparts had both soft and hard band detections but no optical spectral information. We estimate column densities for these assuming various redshifts. At $z = 0$, four of the nine sources would be obscured with $N_{\text{H}} > 10^{22} \text{ cm}^{-2}$. At $z = 1$, seven sources would be obscured, and at $z = 2$, eight sources would show obscuration, though none Compton-thick. The ninth source, which does not show obscuration, is a very bright, nearby galaxy with a hardness ratio of -0.46 . This source is likely a normal galaxy and is further discussed in Section 4.2.

⁹Column densities were estimated using PIMMS (Portable, Interactive Multi-Mission Simulator; Mukai 1993) v3.9b to convert between X-ray source fluxes and count rates.

4.1.1. X-Ray Stacking

For the sources without X-ray detections we use a stacking analysis to search for traces of X-ray emission (see Georgakakis et al. 2008). Removing sources outside the *Chandra* field and sources too close to a bright, potentially contaminating neighbor yielded 39 stackable sources. Stacking the counts from the 39 undetected sources yielded significant detections ($> 3\sigma$) in both the hard and soft bands. The mean hard band flux of the stacked galaxies is $(1.55 \pm 0.50) \times 10^{-16}$ ergs cm^{-2} s^{-1} and the mean soft band flux is $(3.73 \pm 0.87) \times 10^{-17}$ ergs cm^{-2} s^{-1} . These fluxes are near the detection limit of the 2Ms CDF-N, and deeper observations in the EGS would likely have detected more of these stacked sources. However, the average fluxes indicate that as many as half of these sources would not have been detected at the catalog limits even in the deepest existing X-ray survey. The work of Donley et al. (2005, 2007) suggests that most would be weakly detectable ($\geq 2\sigma$) in the deepest surveys, with a minority well below even these limits.

The stacked source has a hardness ratio of -0.11 ± 0.20 corresponding to an effective X-ray spectral slope $\Gamma = 1.2$, which is slightly harder than the $\Gamma = 1.4$ observed for the X-ray background. Assuming a redshift $z = 1$, the observed hardness ratio corresponds to a moderately obscured column density of $\sim 4 \times 10^{22}$ cm^{-2} .

The distribution of detected counts in the stacked signal indicates that the emission is not dominated by a small sample of sources, but is representative of the overall undetected population as a whole. These results are for the combined sample; repeating the analysis for the undetected flux-cut and q -selected sources separately yields roughly similar spectra and fluxes, though the flux-cut sample is slightly harder with $\text{HR} = -0.05$ (corresponding to an effective $\Gamma = 1.1$), as opposed to $\text{HR} = -0.15$ (corresponding to an effective $\Gamma = 1.3$) for the q -selected sample.

The results of the stacking analysis suggest that the undetected sources may be faint or moderately obscured AGNs. However, the spectral slopes are too uncertain to accurately determine the fraction of Compton thick sources in our sample.

4.2. Optical Properties

Eight of the 72 candidates have associated DEEP2 spectra, six from the q -selected sample and two from the flux-cut sample. Two q -selected sources (33%) and one flux-cut source (50%) show optical signatures of AGNs, with broad emission lines and/or strong absorption features indicative of outflows. All three of these optically identified AGNs also have X-ray counterparts. One optical source fits the spectrum of a normal massive elliptical

galaxy. The rest show either no optical spectral features, or features resembling star-forming systems. If these objects are AGNs, our selection criteria find sources that mostly have no optical AGN signatures and may be part of the obscured population.

Four q -selected sources have spectroscopic redshifts ranging from 0.89 to 1.41 with a mean of $z \sim 1$. Two sources from the flux-cut sample have spectroscopic redshifts, both near $z \sim 1$. Assuming the $3.6 \mu\text{m}$ emission is largely dominated by the old stellar population rather than AGN light, we can roughly estimate the photometric redshift of the remaining sources using the $K-z$ relation for radio galaxies (Willott et al. 2003). With our assumption, the $3.6 \mu\text{m}$ flux densities are upper limits to those at K , so the flux densities for the IRAC-detected sources imply redshifts $z \geq 0.5$. If there is an AGN contribution at $3.6 \mu\text{m}$ (e.g., the power law sources discussed below), then the estimated redshifts become lower limits. If we assume similar host galaxies for the flux-cut sample, the selection limit $S_{3.6 \mu\text{m}} < 45 \mu\text{Jy}$ yields expected redshifts $z \gtrsim 1$. Martínez-Sansigre et al. (2005) adapt the $K-z$ relation to define an $S_{3.6 \mu\text{m}}-z$ correlation which predicts $z \gtrsim 1.4$ for the flux-cut sample.

The hard X-ray/optical R band emission ratio (X/O; see Figure 3) is a diagnostic widely used to separate AGNs from starburst galaxies (Maccacaro et al. 1988; Alexander et al. 2001). Normal galaxies tend to have very weak hard X-ray emission and thus very small X/O ratios. However, AGNs are able to fuel energetic X-rays and are expected to have X-ray to optical ratios of $\sim 0.1-10$. An X/O ratio of $0.01-0.1$ is indicative of lower luminosity AGNs or galaxies dominated by star-formation. Of the 12 candidate sources with hard X-ray and R band detections in our sample, 10 have $X/O > 0.1$, and 8 have $X/O > 1$. Two sources in our sample have extreme X-ray to optical emission ratios > 10 . In the general population of sources with X-ray and optical detections, we found that only 55% of sources had $X/O > 1$. However, our sample sizes are too small to draw statistically significant conclusions between our candidates and the general population. Figure 3 shows the expected X/O ratios from the stacked signals; their positions are consistent with the sources being AGNs rather than starbursts.

One q -selected source, mentioned in Section 4.1, has a very small X/O ratio and is extremely bright in the optical with $R = 16.1$. The hard X-ray flux is $F_{2-10 \text{ keV}} = 1.0 \times 10^{-14}$ ergs $\text{cm}^{-2} \text{s}^{-1}$. This source is the only X-ray source that does not show obscuration. It is not plotted in Figure 3 as it is three orders of magnitude brighter in R than the brightest source in the figure. The X/O ratio of this source and the soft hardness ratio suggest that the X-ray emission may be dominated by X-ray binaries and hot gas in a normal galaxy rather than an active nucleus (Hornschemeier et al. 2003).

4.3. Infrared Properties

Figure 2 plots the hard X-ray flux of the X-ray detected sources against the $24\ \mu\text{m}$ flux density. Half of the detected sources lie in the designated AGN region for local galaxies as determined observationally by Piccinotti et al. (1982) while the other half are in the transition region. The stacked signal is also in the transition region, though close to the local starbursts. Though we have not corrected our sources for redshift, Alexander et al. (2001) show that the observed hard X-ray to mid-IR flux ratio will minimally change with increasing redshift for sources with low column densities and will increase more noticeably for obscured AGNs.

Many AGNs can also be described by their characteristic negative power-law spectral energy distributions (SEDs) which extend from mid-IR to ultraviolet wavelengths: $f_\nu \propto \nu^\alpha$, with $\alpha < -0.5$ (Elvis et al. 1994, see also Alonso-Herrero et al. 2004 and Barmby et al. 2006). This emission can arise from multiple source components near the dusty nucleus that broaden the SED rather than from a single power-law source (e.g. Rieke & Lebofsky 1981). In the IRAC bands, stellar-dominated objects will either exhibit positive (blue) power-law behavior with $\alpha \sim +2$ corresponding to the Rayleigh-Jeans tail of the blackbody spectrum or else not fit a power law at all due to their $8\ \mu\text{m}$ PAH emission or $1.6\ \mu\text{m}$ stellar bump. A number of q -selected sources lie outside the IRAC observed field or lack detections in all four IRAC bands, leaving a sample of 53 out of 72 candidates for which we could study IRAC power-law properties. Ten of these (19%) are well fit to a power law between $3.6\ \mu\text{m}$ and $8.0\ \mu\text{m}$ with $\alpha < -0.5$. Examples of such fits can be found in Alonso-Herrero et al. (2006), Barmby et al. (2006), and Donley et al. (2007). The detection rate is approximately the same for both selection methods, and is comparable to the fraction of X-ray sources with similar power-law slopes in the EGS. Donley et al. (2007) show that the majority of power-law galaxies in the CDF-N lie at high redshifts. The low fraction of power-law detection may be due to the fact that most of our sample are q -selected galaxies, which are predicted to be at low-moderate redshifts.

In a random sample of 53 IRAC sources, we would expect ~ 2 sources to exhibit negative IR power-law behavior based on the numbers found for the entire IRAC population. The Poisson probability of finding 10 or more such power-law sources, as we have done, is only 10^{-4} . Of the general sample of 321 sources with radio, MIPS and IRAC detections, 23 have IRAC power-laws. Thus, the overlap between our sample and the mid-IR power-law sample is substantial, and suggests that both methods are effective at finding AGNs, but the populations found are distinct enough to make both methods necessary.

5. SUMMARY AND DISCUSSION

We have selected 72 AGN candidates by combining and comparing two sets of radio and mid-IR selection criteria. The q -selection method finds 47 sources with 1.4 GHz flux densities far in excess of their 24 μm flux densities, relative to star-forming galaxies. The flux-cut method selects 28 sources based on their 3.6 μm , 24 μm , and 1.4 GHz flux densities. Only three sources overlap in the two methods, since they are designed to probe different redshifts and obscuration levels. This selection is independent of typical selection techniques such as X-ray or optical identifications, and thus we can test the completeness of current AGN samples by finding AGNs missed at other wavelengths.

AGNs are often defined via their mid-IR power-law behavior, optical broad lines, and X-ray detections. Nineteen sources (30%) in our sample have X-ray detections with Poisson false probabilities $< 10^{-3}$ at the *Chandra* 200 ks depth. Column density estimates of the X-ray detected sources indicate that even assuming $z = 0$, half of our sources would be obscured with $N_{\text{H}} > 10^{22} \text{ cm}^{-2}$. The obscuration fraction will increase with redshift. If we assume our sources are at $z = 1$, which is the mean value determined from the few sources with spectroscopic data, nearly all of the X-ray detected sources are obscured. Among the X-ray undetected sample, stacking techniques demonstrate low but significant levels of X-ray activity above the background emission. The stacked source has $\Gamma = 1.2$, which is slightly flatter (harder) than the general X-ray background. The relatively high X-ray detection fraction and the properties of the stacked source indicate that we are finding a population of moderately obscured, though not Compton-thick, previously undetected AGNs. The rate of X-ray confirmation of AGN status is a function of the depth of the observations, and future work in this area will benefit from recently awarded additional *Chandra* pointings in the field.

The radio/mid-IR selected sample also finds more sources separately defined as AGNs via their optical or infrared properties than a random selection from the parent sample. However, our sample is also distinct from AGNs found using these other selection techniques: less than 20% exhibit the IRAC power-law behavior expected of luminous AGNs (e.g., Donley et al. 2007), and 38% show AGN signatures in their optical spectra. Table 1 summarizes the numbers of AGNs identified by each technique separately for the flux-cut and q -selected samples. Accounting for the overlap in multi-wavelength AGN identification for some sources, 60% of our candidates have not been identified as AGNs via optical spectra, IRAC power-laws, or X-ray detections. The selection criteria used here thus contribute to a more complete census of AGNs, and a variety of selection techniques, requiring study at all wavelengths, are required in order to find the least biased samples of AGNs.

Compared to our X-ray detection rate of 30%, Donley et al. (2005) detected 80% (40%)

of the candidates in their q -selected sample at 2σ (5σ) in the deeper CDF-N, while Martínez-Sansigre et al. (2007) detected $\gtrsim 5\%$ in the shallower SXDF with a flux limit of $F_{2-12 \text{ keV}} = 3 \times 10^{-15}$ ergs $\text{cm}^{-2} \text{ s}^{-1}$. In general, the flux-cut method finds a greater proportion of AGNs not identified via other wavelengths than the q -selected sources. This may be due to a greater fraction of obscured sources in the sample, as indicated by their stacked signal being slightly harder than the q -selected stacked signal. Also, the flux-cut sample is much fainter at X-ray and optical wavelengths and AGN activity may be too faint to detect in X-rays (either intrinsically, or due to larger redshifts) or hidden by host galaxy light at optical wavelengths. However, it is also possible that the flux-cut sample simply has a higher rate of contamination from starforming systems, and thus a smaller fraction of confirmed AGNs.

Both of the selection techniques we apply find only sources that are either moderately radio-loud or occupy the bright end of the radio-quiet population (Ivezić et al. 2002). Radio-loud sources are expected to make up only $\sim 10 - 20\%$ of the total AGN population (Kellermann et al. 1989; Urry & Padovani 1995; Ivezić et al. 2002), so 80-90% of AGNs are undetected with these techniques. Sixty per cent of our candidates remained undetected using other AGN identification techniques. If we assume that under the unified model of AGNs, the central engine behaves the same for both radio-loud and radio-quiet sources, we can estimate that the same fraction of radio quiet sources are undetected by these other methods. This implies that half of the overall AGN population has yet to be found, and novel techniques must be developed in order to obtain a complete sample of AGNs.

We are grateful to the referee for comments that helped improve this paper. This work is based in part on observations made with the Spitzer Space Telescope, which is operated by the Jet Propulsion Laboratory, California Institute of Technology under a contract with NASA. Support for this work was provided by NASA. This work is based in part on data collected at Subaru Telescope, which is operated by the National Astronomical Observatory of Japan. ESL acknowledges support from STFC. AG acknowledges funding from the Marie-Curie Fellowship grant MEIF-CT-2005-025108. ALC is supported by NASA through Hubble Fellowship grant HF-01182.01-A, awarded by the Space Telescope Science Institute, which is operated by the Association of Universities for Research in Astronomy, Inc., for NASA, under contract NAS 5-26555.

Facilities: CFHT, CXO, Keck:II, Spitzer (IRAC, MIPS), Subaru (Suprime), VLA

REFERENCES

Alexander, D. M., et al. 2001, ApJ, 554, 18

- Alexander, D. M., Brandt, W. N., Hornschemeier, A. E., Garmire, G. P., Schneider, D. P., Bauer, F. E., & Griffiths, R. E. 2001, *AJ*, 122, 2156
- Alonso-Herrero, A., et al. 2004, *ApJS*, 154, 155
- Alonso-Herrero, A., et al. 2006, *ApJ*, 640, 167
- Appleton, P. N., et al. 2004, *ApJS*, 154, 147
- Barmby, P., et al. 2006, *ApJ*, 642, 126
- Barmby, P., et al. 2008, *ApJS*, submitted
- Biggs, A. D., & Ivison, R. J. 2006, *MNRAS*, 371, 963
- Brand, K., et al. 2006, *ApJ*, 644, 143
- Boyle, B. J., Cornwell, T. J., Middelberg, E., Norris, R. P., Appleton, P. N., & Smail, I. 2007, *MNRAS*, 376, 1182
- Coil, A. L., Newman, J. A., Kaiser, N., Davis, M., Ma, C.-P., Kocevski, D. D., & Koo, D. C. 2004, *ApJ*, 617, 765
- Comastri, A., Fiore, F., Vignali, C., Matt, G., Perola, G. C., & La Franca, F. 2001, *MNRAS*, 327, 781
- Condon, J. J. 1992, *ARA&A*, 30, 575
- Daddi, E., et al. 2007, *ArXiv e-prints*, 705, arXiv:0705.2832
- Davis, M., et al. 2003, *Proc. SPIE*, 4834, 161
- Davis, M., et al. 2007, *ApJ*, 660, L1
- Donley, J. L., Rieke, G. H., Rigby, J. R., & Pérez-González, P. G. 2005, *ApJ*, 634, 169
- Donley, J. L., Rieke, G. H., Pérez-González, P. G., Rigby, J. R., & Alonso-Herrero, A. 2007, *ApJ*, 660, 167
- Elvis, M., et al. 1994, *ApJS*, 95, 1
- Engelbracht, C. W., et al. 2007, *PASP*, 119, 994
- Fadda, D., Flores, H., Hasinger, G., Franceschini, A., Altieri, B., Cesarsky, C. J., Elbaz, D., & Ferrando, P. 2002, *A&A*, 383, 838

- Fazio, G. G., et al. 2004, *ApJS*, 154, 10
- Fiore, F., et al. 2007, *ArXiv e-prints*, 705, arXiv:0705.2864
- Georgakakis, A., et al. 2008, *MNRAS* in press, *ArXiv e-prints*, 801, arXiv:0801:2160
- Gilli, R., Comastri, A., & Hasinger, G. 2007, *A&A*, 463, 79
- Hornschemeier, A. E., et al. 2003, *AJ*, 126, 575
- Ivezić, Ž., et al. 2002, *AJ*, 124, 2364
- Ivison, R. J., et al. 2007, *ApJ*, 660, L77
- Jiang, L., Fan, X., Ivezić, Ž., Richards, G. T., Schneider, D. P., Strauss, M. A., & Kelly, B. C. 2007, *ApJ*, 656, 680
- Kellermann, K. I., Sramek, R., Schmidt, M., Shaffer, D. B., & Green, R. 1989, *AJ*, 98, 1195
- Kovács, A., Chapman, S. C., Dowell, C. D., Blain, A. W., Ivison, R. J., Smail, I., & Phillips, T. G. 2006, *ApJ*, 650, 592
- Lacy, M., et al. 2004, *ApJS*, 154, 166
- Laird, E. S., Nandra, K., Hobbs, A., & Steidel, C. C. 2006, *MNRAS*, 373, 217
- Maccacaro, T., Gioia, I. M., Wolter, A., Zamorani, G., & Stocke, J. T. 1988, *ApJ*, 326, 680
- Martínez-Sansigre, A., Rawlings, S., Lacy, M., Fadda, D., Marleau, F. R., Simpson, C., Willott, C. J., & Jarvis, M. J. 2005, *Nature*, 436, 666
- Martínez-Sansigre, A., et al. 2007, *MNRAS*, 379, L6
- Mukai, K. 1993, *Legacy*, 3, 21
- Mushotzky, R. 2004, *Supermassive Black Holes in the Distant Universe*, 308, 53
- Nandra, K., George, I. M., Mushotzky, R. F., Turner, T. J., & Yaqoob, T. 1997, *ApJ*, 477, 602
- Nandra, K., 2008, in prep
- Piccinotti, G., Mushotzky, R. F., Boldt, E. A., Holt, S. S., Marshall, F. E., Serlemitsos, P. J., & Shafer, R. A. 1982, *ApJ*, 253, 485
- Ranalli, P., Comastri, A., & Setti, G. 2003, *A&A*, 399, 39

- Rieke, G. H., & Lebofsky, M. J. 1981, *ApJ*, 250, 87
- Rieke, G. H., et al. 2004, *ApJS*, 154, 25
- Risaliti, G., Maiolino, R., & Salvati, M. 1999, *ApJ*, 522, 157
- Seymour, N., et al. 2007, *MNRAS*, submitted
- Stern, D., et al. 2005, *ApJ*, 631, 163
- Szokoly, G. P., et al. 2004, *ApJS*, 155, 271
- Treister, E., et al. 2005, *ApJ*, 621, 104
- Ueda, Y., Akiyama, M., Ohta, K., & Miyaji, T. 2003, *ApJ*, 598, 886
- Urry, C. M., & Padovani, P. 1995, *PASP*, 107, 803
- Vlahakis, C., Eales, S., & Dunne, L. 2007, *MNRAS*, 379, 1042
- Weedman, D. W., Le Floch, E., Higdon, S. J. U., Higdon, J. L., & Houck, J. R. 2006, *ApJ*, 638, 613
- Werner, M. W., et al. 2004, *ApJS*, 154, 1
- Willott, C. J., Rawlings, S., Jarvis, M. J., & Blundell, K. M. 2003, *MNRAS*, 339, 173
- Worsley, M. A., et al. 2005, *MNRAS*, 357, 1281
- Wu, H., Cao, C., Hao, C.-N., Liu, F.-S., Wang, J.-L., Xia, X.-Y., Deng, Z.-G., & Young, C. K.-S. 2005, *ApJ*, 632, L79
- Yun, M. S., Reddy, N. A., & Condon, J. J. 2001, *ApJ*, 554, 803

Table 1. Comparison of Selection Techniques

	Number in Sample	X-ray Detection	IRAC Power-law Detection	Optically Identified AGN Spectra
Flux-Cut	28	4/26	5/26	1/2
<i>q</i> -Selected	47	15/37	6/28	2/6
Total	72	19/61	10/53	3/8

Note. — The first column gives the number of sources selected with the radio/mid-IR methods outlined in this paper. The subsequent columns indicate the number of sources from our candidate list identified as AGNs via other selection techniques and the number of sources detected in the relevant parent sample.

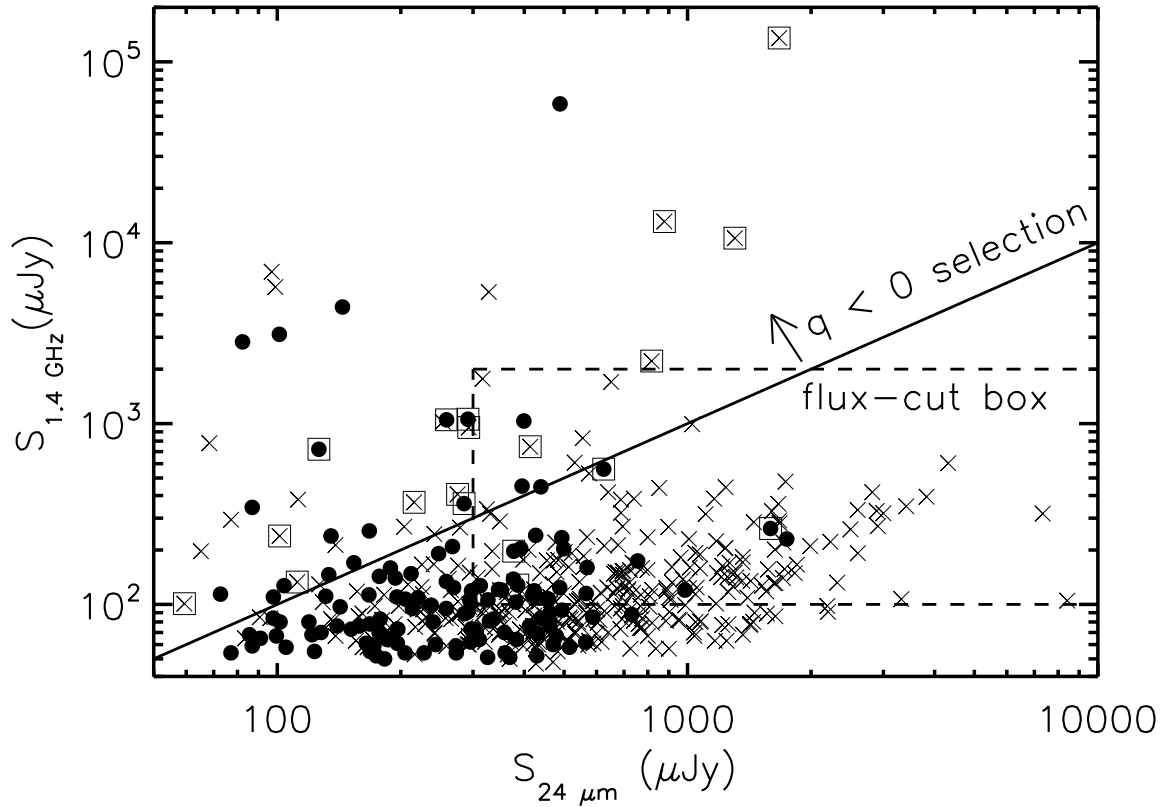


Fig. 1.— Selection Criteria. All sources with both 24 μm and 1.4 GHz detections are plotted; dots represent sources with $S_{3.6 \mu\text{m}} \leq 45 \mu\text{Jy}$, all other sources are depicted by crosses. AGN candidate sources with X-ray detections have been overplotted with squares. The flux-cut method selects all the dots within the dashed selection box; the q -selection method selects all sources above the solid line (dots and crosses).

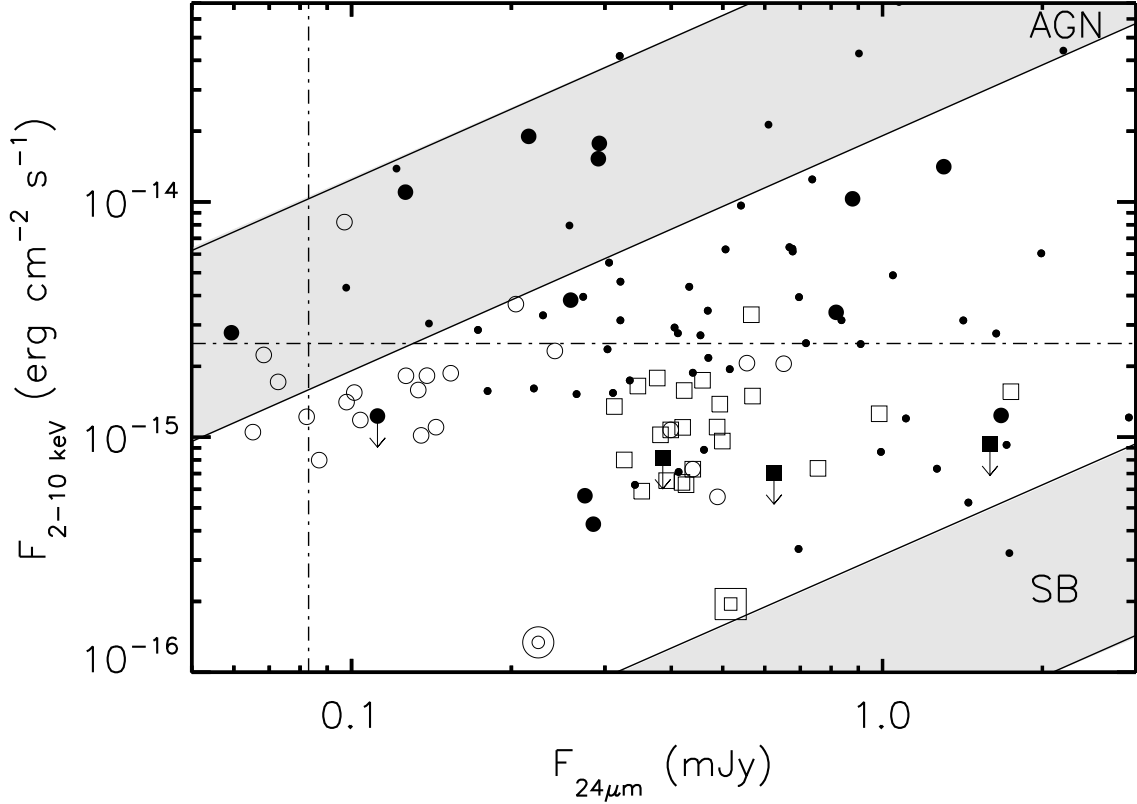


Fig. 2.— $24 \mu\text{m}$ emission vs. the hard $2 - 10 \text{ keV}$ X-ray fluxes for the sample of radio detected sources. Squares/large circles represent the flux-cut/ q -selected sources. All other hard X-ray sources with $24 \mu\text{m}$ detections in the field are depicted by small dots. Filled symbols denote sources with X-ray detections while open symbols indicate hard X-ray upper limits for the non-detected sources. Filled symbols with arrows represent upper limits for sources detected in the X-ray, but not in the hard band. All open symbols without arrows are X-ray upper limits; down-facing arrows were not plotted for clarity. The two stacked circles/squares represent the hard band flux of the stacked signals and the mean $24 \mu\text{m}$ emission of the stacked sources. The horizontal line represents the flux to which 80% of the X-ray survey area is sensitive, and the vertical line is the 80% completeness limit for MIPS. Extrapolated regions for local AGNs and starburst galaxies are overplotted (Piccinotti et al. 1982; Ranalli et al. 2003; Alonso-Herrero et al. 2004).

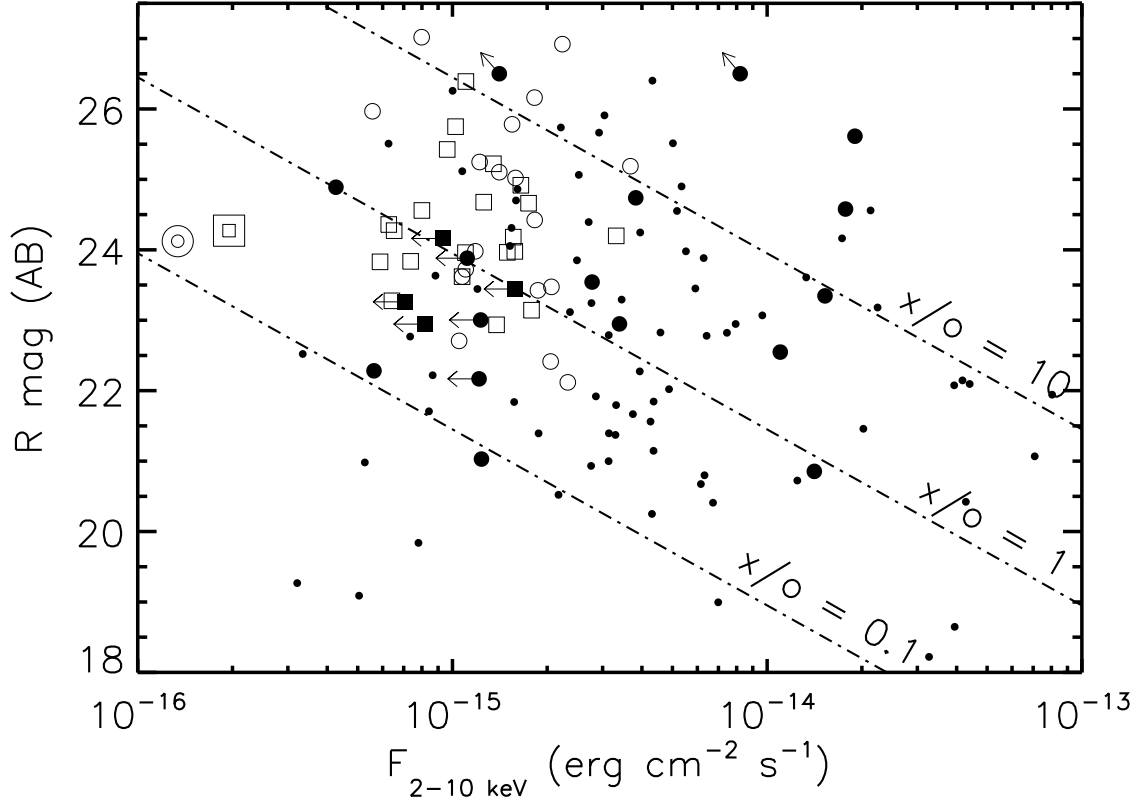


Fig. 3.— Hard X-ray (2 – 10 keV) fluxes vs. R band magnitudes. Squares/large circles represent the flux-cut/ q -selected sources. All other hard X-ray sources with R band detections in the field are depicted by small dots. Filled symbols denote sources with X-ray detections while open symbols indicate hard X-ray upper limits for the non-detected sources. Filled symbols with arrows represent upper limits for sources detected in the X-ray, but not in the hard band. Symbols with arrows pointing upper left depict candidates without firm detections in either hard X-rays or R band. All open symbols without arrows are X-ray upper limits; left-facing arrows were not plotted for clarity. The two stacked circles/squares represent the hard band flux of the stacked signals and the mean R band emission of the stacked sources. Diagonal lines represent constant value X/O ratios. AGNs are expected to lie above $X/O > 0.1$ (Hornschemeier et al. 2003)